Ising-type quasi-one-dimensional ferromagnetism with anisotropic hybridization in UNi_4P_2

Arvind Maurya,[1,2,*] Atsushi Miyake,[3] Hisashi Kotegawa,[4] Yusei Shimizu,[2] Yoshiki J. Sato,[2] Ai Nakamura,[2] Dexin Li,[2] Yoshiya Homma,[2] Fuminori Honda,[2,5] Masashi Tokunaga,[3] and Dai Aoki[2]

[1]*Department of Physics, School of Physical Sciences, Mizoram University, Aizawl 796 004, India*
[2]*Institute for Materials Research, Tohoku University, Oarai, Ibaraki 311-1313, Japan*
[3]*Institute for Solid State Physics, The University of Tokyo, Kashiwa, Chiba 277-8581, Japan*
[4]*Department of Physics, Kobe University, Kobe 658-8530, Japan*
[5]*Central Institute of Radioisotope Science and Safety Management, Kyushu University, Motooka 744, Fukuoka Nishi, Fukuoka 819-0395, Japan*

(Received 14 January 2022; revised 30 January 2023; accepted 31 January 2023; published 24 February 2023)

We report single-crystal growth and demonstrate Ising-type ferromagnetism with a Curie temperature of 25 K in UNi_4P_2 by means of magnetization, electrical transport, and specific heat measurements. Uniaxial anisotropy in magnetism and cf hybridization are well reflected not only in the crystallographic ac plane but also within the basal plane of the tetragonal unit cell owing to the quasi-one-dimensional crystal and electronic structure of UNi_4P_2. The strong anisotropy between the c axis and the tetragonal basal plane is retained up to 57 T, while the intraplane anisotropy in the basal plane gradually vanishes at higher fields. Our results show that anisotropic electron correlations may stabilize the elusive Ising-type ferromagnetic order in one dimension at nonzero temperatures, presumably with its own characteristic universality class.

DOI: 10.1103/PhysRevB.107.085142

Strong spin-orbit coupling together with the semi-itinerant nature of $5f$ electrons is believed to seed exclusive ground states in actinide compounds. Ferromagnetic superconductors, spin-triplet superconductors, and hidden-order materials are some of the extraordinary material classes mainly composed of uranium compounds. A trio of archetypal ferromagnetic superconductors, UGe_2, URhGe, and UCoGe [1], have attracted many researchers for more than two decades, while a consensus on the order parameter of the hidden thermodynamic phase in URu_2Si_2 [2] is yet to be reached after gigantic efforts by generations of experimental and theoretical condensed matter physicists over more than three decades. A revisit of correlated electron uranium compounds is promising for discovering similar or novel electronic orders. For example, recently discovered topological triplet superconductivity close to multiple instabilities (magnetic and Fermi surface) in UTe_2 has rejuvenated the inspiration for finding ferromagnetic superconductors [3,4]. Likewise, a hidden-order-like situation may potentially be realized in other materials, e.g., in URhSn [5]. Notably, our recent work has surfaced field boosting of the undetermined order parameter in URhSn [5] and an exotic kind of quantum phase transition, one of its kind, which involves a pair of bicritical points at the same pressure (6.25 GPa) with low-temperature ferromagnetic phases composed of the ordered phases in localized and itinerant electron scenarios of quantum criticality [6].

Categorically, the reduced dimensionality in the electronic structure is believed to stabilize the elusive ferromagnetic quantum critical point in $YbNi_4P_2$ after 10% atomic substitution of P by As [7]. Owing to the low Curie temperature (170 mK), it is easy to suppress T_{Curie} in $YbNi_4P_2$; however, by the same token, the study of anisotropic magnetism in the ordered state is challenging. Herein, we have systematically studied the anisotropy in a ferromagnet UNi_4P_2 by means of magnetization and electrical resistivity complemented by the heat capacity, which is isostructural with $YbNi_4P_2$ but exhibits a rather large Curie temperature.

In exploratory actinide materials, at first sight, $5f$-orbital-derived ferromagnets, particularly those with weak entropy change associated with the magnetic order, are promising. Although a ferromagnetic order at 21 K is reported in polycrystalline UNi_4P_2 [8], single-crystal growth and anisotropy in physical properties hitherto have not been studied. Possible hurdles could be the high vapor pressure and corrosive nature of phosphorus and the inability to stabilize the desired phase in commonly used low-melting-point metal solvents, e.g., Sn, In, Bi, and Pb, as we learned from our previous unsuccessful attempts. Eventually, we succeeded in growing high-quality large single crystals by using a eutectic composition of Ni and P as a self-flux, enabling us to explore anisotropic magnetic and electronic properties by means of magnetization, specific heat, and electrical resistivity measurements.

The crystal structure of UNi_4P_2 is $ZrFe_4Si_2$-type tetragonal with space group $P4_2/mnm$ (No. 136), as shown in Fig. 1(a) [8,9]. Linear chains of uranium atoms and edge-shared distorted tetrahedral units of Ni atoms along the [001] direction impart one dimensionality in the crystal structure, which translates into platelike Fermi sheets in the electronic structure [7,9,10]. A lack of of direct overlap between $5f$ orbitals for next-nearest U atoms owing to the intermediate blocks of Ni_4-

*arvindmaurya.physics@gmail.com

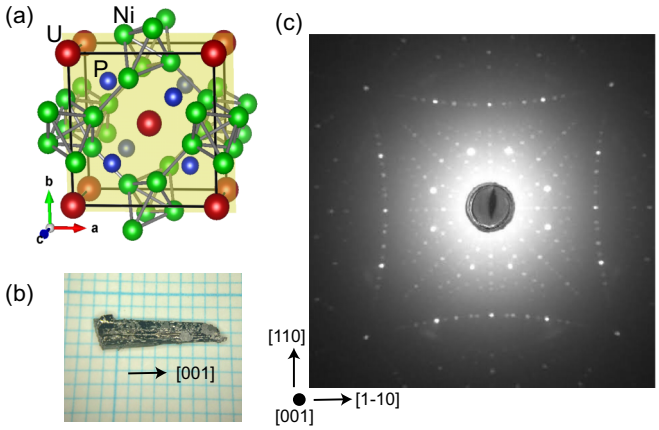

FIG. 1. (a) Crystal structure of UNi_4P_2, (b) a typical flux-grown single crystal of UNi_4P_2 placed on graph paper with millimeter grid, and (c) Laue diffraction pattern of UNi_4P_2. U atoms lie at the corners and at the body-center position, and edge-shared distorted tetragonal units of Ni atoms form a chain along the c axis, while pairs of phosphorus atoms lie in the diagonal directions of the basal plane alternatively at $c = 0$ and $c = 1/2$, respectively. The yellow-shaded mirror plane in (a) contains one pair of phosphorus atoms located diagonally in the square basal plane, while another pair of P atoms lie in the perpendicular direction in a parallel plane at $c/2$ distance.

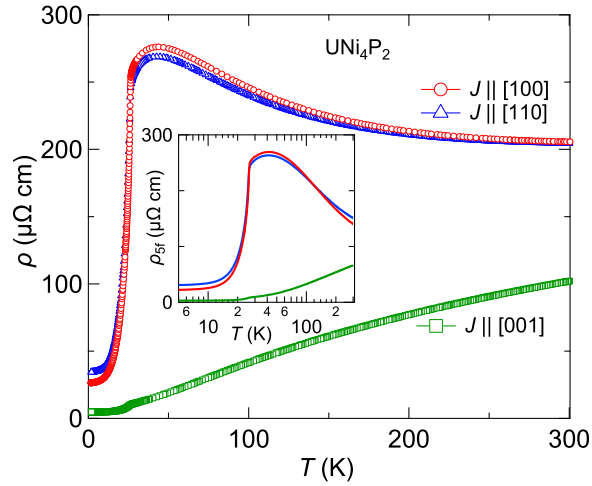

FIG. 2. Electrical resistivity as a function of temperature $[\rho(T)]$ in UNi_4P_2 depicting anisotropic cf hybridization and Fermi surface owing to a significant difference between lattice constants a and c. The inset shows the $-\ln T$ slope apparent in ρ_{5f} $[= \rho(T) - \rho_{LuNi_4P_2}(T)]$ when current is passed along the basal plane.

polyhedral chains further supports one dimensionality with a potential to furnish enhanced quantum mechanical effects in UNi_4P_2. The shortest U-U distance is along the chain direction, i.e., [001] length is 3.65 Å.

Firstly, a polycrystalline ingot of UNi_4P_2 was prepared by arc-melting uranium with prereacted Ni_2P. A eutectic composition Ni : P = 81 : 19 was used as a self-flux with polycrystalline UNi_4P_2 at molar ratio 19 : 1. A slow cooling from 1100 to 930 °C at a rate of 1 °C/h resulted in large single crystals with the maximum size limited by the crucible dimension [Fig. 1(b)]. Canfield crucibles (LSP Industrial Ceramics) with a fritted sandwiching lid facilitated a clean removal of the excess flux at 930 °C in a single heating cycle. The starting ingredients were sealed in a quartz ampoule, first evacuating the pressures below 10^{-6} Torr and then adding inert argon gas up to a partial pressure equal to the atmospheric pressure at elevated temperatures. As another safety measure for the risk associated with the high vapor pressure of phosphorus, a slow heating at a rate of 15 °C/h was implemented in the prereaction of the Ni_2P alloy as well as in the flux growth. Our procedure not only yields high-quality large single crystals of UNi_4P_2 but also takes less time than polycrystalline synthesis, which requires annealing at 1000 °C for 2 months in order to get a single phase [8].

Laue diffraction [Fig. 1(c)] of the flux-grown crystals confirmed a tetragonal needle morphology with large (110) facets and length along [001]. A thin layer of flux firmly stuck on the crystal surfaces was removed by mechanical polishing and a spark cutter. Electron dispersive spectroscopy, powder x-ray diffraction, and single-crystal diffraction concurrently confirmed the desired phase. A similar procedure also gives single crystals of a nonmagnetic isostructural Lu analog; however, the yield and size of the crystals are smaller compared with UNi_4P_2. We confirmed the absence of superconductivity in $LuNi_4P_2$ down to 150 mK.

Electrical resistivity, specific heat, and magnetization up to 5 T were measured in commercial physical and magnetic property measurement systems (PPMS and MPMS), respectively. High-field magnetization up to 57 T was measured in a pulsed-field magnet by the induction method.

The temperature dependence of the electrical resistivity $[\rho(T)]$ of UNi_4P_2 is remarkably anisotropic between the c direction and the perpendicular plane. Figure 2 $\rho(T)$ curves in the basal plane show a negative slope accompanied by a broad maximum around 40 K, reflecting a hybridization between $5f$ orbitals and conduction band electrons (cf hybridization), and a sharp drop below T_{Curie} owing to the loss of spin-disorder scattering. The electrical resistivity component contributed by U-$5f$ electrons (ρ_{5f}) in UNi_4P_2 is obtained by subtraction of the phonon resistivity as estimated by $LuNi_4P_2$ from the $\rho(T)$, in which $-\ln T$ behavior is pronounced in the basal plane (inset of Fig. 2). However, the response for $J \parallel c$ is different even qualitatively, revealing less enhancement of resistivity due to the hybridization effect and a smaller spin-disorder contribution. Emphatically, the Kondo effect is a hallmark of the cf hybridization in f-electron systems [11,12]. The plate-like Fermi surface in the ab plane [9] provides a larger density of conduction electrons in the basal plane in the tetragonal symmetry, which are anisotropically available for hybridizing with the $5f$ electrons, naturally consistent with the anisotropic Kondo effect experimentally observed in UNi_4P_2.

A large anisotropy is also apparent in the residual resistivity ratio (RRR), residual resistivity ρ_0, and quadratic temperature coefficient (A coefficient) extracted after fitting $\rho = \rho_0 + AT^2$ in the temperature range 2–4 K (Table I). Note that ρ_0 and the A coefficient in the basal plane are an order of magnitude larger than those along the [001] direction, further supporting a strongly anisotropic cf hybridization owing to reduced dimensionality in UNi_4P_2. Following electrical transport, the magnetization behavior is highly anisotropic,

TABLE I. Anisotropy in magnetic and transport properties in UNi_4P_2.

Direction	A ($\mu\Omega$ cm K^{-2})	ρ_0 ($\mu\Omega$ cm)	RRR	$\mu_{\rm eff}$ (μ_B/f.u.)	θ_p (K)	χ_0 (10^{-3} emu mol^{-1})	M(2 K, 1 T) (μ_B/f.u.)	χ(at 2 K, between 2 T to 1 T) (10^{-3} emu mol^{-1})
[100]	0.032	27	8	1.96 ± 0.02	39 ± 6	1.12	0.85	1.43
[110]	0.028	34	6	1.92 ± 0.01	39 ± 1	1.16	0.60	12.40
[001]	0.0007	4.7	22				0.01	27.88

particularly at low temperatures well inside the ferromagnetic state. Figures 3(a) and 3(b) show the magnetization along directions [100], [110], and [001] between 2 K and 300 K measured in 1 T magnetic field and the isothermal magnetization at 2 K, respectively. The anisotropy in $M(T)$ can be readily seen all over the measured temperature range. In the ordered state, in the low-temperature limit, $M(2\ \text{K}, H = 1\ \text{T})$ becomes nearly temperature independent; a similar anisotropic behavior, i.e., $M_{[100]} > M_{[110]} \gg M_{[001]}$, is reproduced in $M(H)$ at $T = 2$ K. Table I lists the Curie-Weiss parameters deduced from high-temperature (300–350 K) inverse susceptibility data, which are nearly isotropic within the basal plane. The paramagnetic effective moment values are slightly reduced but comparable for a uranium $5f$-orbital based magnet (e.g., 2.24 μ_B/f.u. in URuAl) [11], while the paramagnetic Curie temperatures are positive [as expected for a ferromagnetic (FM) ground state] but significantly larger than the Curie temperature. Note that a large magnetocrystalline anisotropy or cf hybridization can be attributed to this deviation [13]. Unphysically large values for $\mu_{\rm eff}$ and θ_p in the [001] direction, due to a large magnetocrystalline anisotropy, are obtained, and hence we omit listing them here. The temperature-independent susceptibility χ_0 is mainly composed of the Pauli susceptibility and Van Vleck susceptibility.

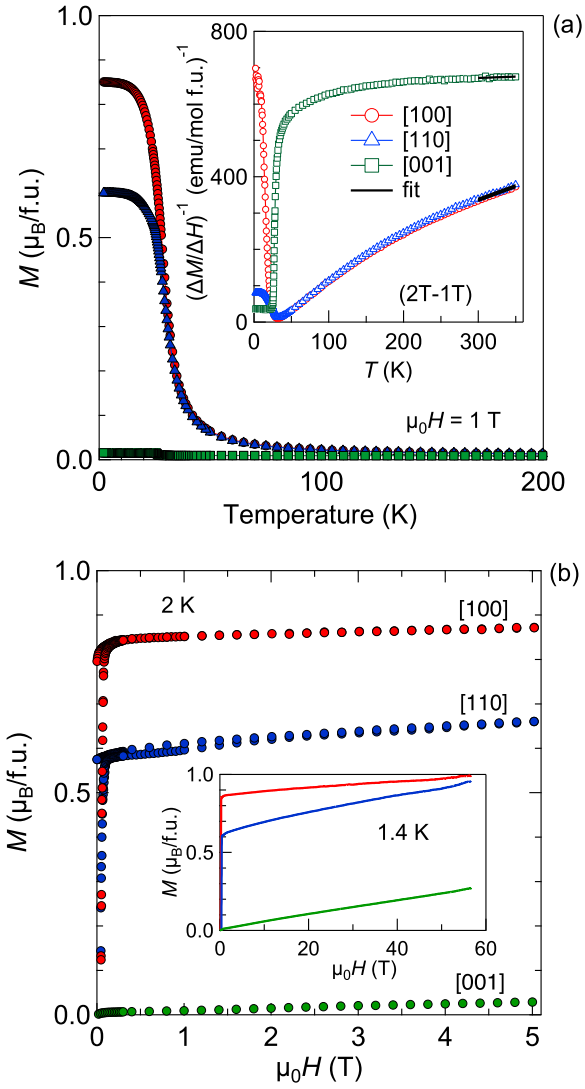

FIG. 3. Anisotropic magnetism in UNi_4P_2. (a) Magnetization and inverse susceptibility (inset) as a function of temperature for $H \parallel$ [100], [110], and [001], respectively. The black curves in the inset are fits of the inverse susceptibility, $\chi^{-1} = (\Delta M/\Delta H)^{-1}$ measured between 1 and 2 T, to Curie-Weiss behavior. (b) Anisotropic $M(H)$ curves in UNi_4P_2 up to 5 T (main panel) measured in the MPMS and up to 57 T (inset) measured in a pulsed-field magnet.

At higher fields the magnetization gradually increases in all directions to attain saturation; however, owing to the high-field susceptibility in [110] being larger than that in [100], the anisotropy within the basal plane gradually vanishes at elevated fields [inset of Fig. 3(b)]. It is also noted that UNi_4P_2 has a large magnetic anisotropy between the basal plane and [001]. It is evident that anisotropic constants, namely, K_1 and K_2, in tetragonal symmetry are large in UNi_4P_2, but extremely intense fields are necessary to determine these anisotropic constants because there is no saturation behavior in the $M(H)$ curve for the hard magnetization axis ($H \parallel$ [001]) even at 57 T.

The anisotropy in the resistivity behavior of UNi_4P_2 is apparently similar to that in the Yb analog, in contrast with the magnetization in the paramagnetic behavior [10]. The ordered moment deduced from back-tracing the saturated $M(H)$ curves at 2 K between 2 and 5 T fields follows a simple projection formula: $\mu_{\rm ord}(\phi) = \mu_{\rm ord}([100])\cos(\phi)$, where ϕ is the angular deviation from the a axis (Fig. 4). Remarkably, the empirical projection rule for the ordered moment is valid for the (100) plane as well as for the (001) plane. This altogether reveals that the magnetic moments point in the [100] direction in UNi_4P_2 with Ising-type ferromagnetic ordering. Note that neither Heisenberg nor XY (nor any other) magnetism can produce this behavior in a tetragonal symmetry. The same behavior is presented as proof of Ising-type anisotropy in Ref. [14].

The magnitude of the ordered moment as inferred by magnetization along [100] is 0.85 μ_B, which is smaller than $\mu_{\rm eff} = 1.92\ \mu_B$. The Rhodes-Wohlfarth ratio [15], p_s/p_c, where p_s is the saturation moment and $p_c = \sqrt{1 + \mu_{\rm eff}^2} - 1$, turns out to be 1.165. A departure from unity shows that the magnetic electrons tend to be itinerant in UNi_4P_2.

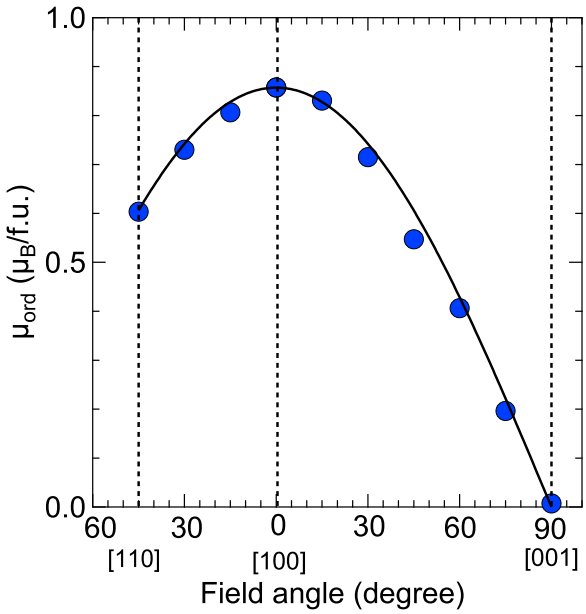

FIG. 4. Ordered moment μ_{ord} derived by extrapolating the slope of the $M(H)$ data between 2 and 5 T at 2 K to 0 T. The solid curve corresponds to the ordered moment with the orientation expected from a simple projection law for Ising-type ferromagnetism.

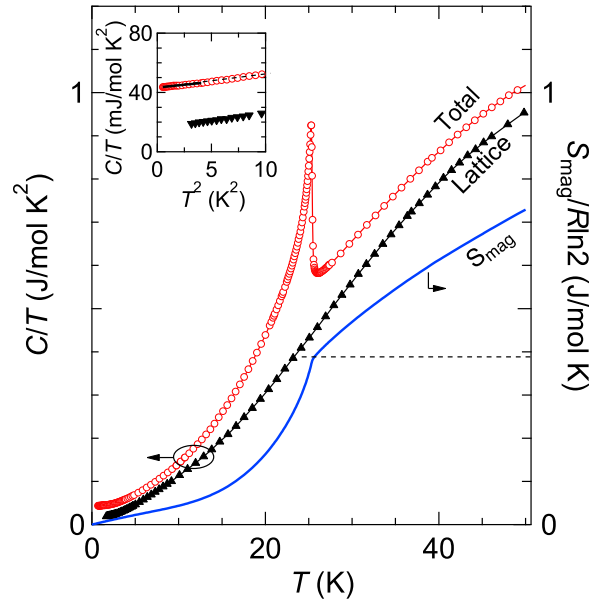

FIG. 5. Specific heat capacity divided by temperature (C/T) on the left axis and magnetic entropy S_{mag} on the right axis with a common temperature scale. The inset shows the low-temperature data with fit (black curve) to derive the γ_{el} value.

Another criterion of itineracy is given by the ratio T_{Curie}/T_O, as described in the framework of Takahashi's spin fluctuation theory [16]. Here, T_O is a temperature parametrizing the width of the spin fluctuation spectrum in the energy space, which is derivable from the isothermal magnetization curve at low temperatures as discussed in detail in Refs. [17,18]. In UNi_4P_2, we deduce $T_O = 54.4$ K from $M(H)$ at 2 K, furnishing $T_{Curie}/T_O = 0.46$. A reduced value of the ratio compared with unity is again consistent with the nearly itinerant nature of the $5f$-orbital electrons in UNi_4P_2. Notably, a systematic study of 79 uranium ferromagnets by Tateiwa *et al.* [17] shows that most of them exhibit itinerant behavior.

In specific heat (Fig. 5), the second-order ferromagnetic phase transition in UNi_4P_2 is depicted by a sharp lambda-type peak at the Curie temperature $T_{Curie} = 25.2$ K with $\Delta C/T(T_{Curie}) = 0.34$ J mol^{-1} K^{-1}. The specific heat of $LuNi_4P_2$ with temperature scale multiplied by the ratio $\sqrt{FW_{LuNi_4P_2}}/\sqrt{FW_{UNi_4P_2}}$, where FW refers to formula weights, provides an estimation of the lattice contribution, which when subtracted from the specific heat of UNi_4P_2 gives the heat capacity contributed by the $5f$ electrons, $C_{mag}(T)$. The integral of $C_{mag}(T)/T$ with temperature results in the magnetic entropy $S_{mag}(T)$ of UNi_4P_2 as shown in Fig. 5 on the scale on the right-hand side. A magnetic entropy of $0.39\,R\ln 2$ is released at T_{Curie}, and a relatively small value is consistent with a cf hybridization and hence weak itinerant nature of the ferromagnetism in UNi_4P_2; here, R is the universal gas constant. Fitting the equation $C/T = \gamma_{el} + \beta_{ph}T^2$ to the specific heat data between 0.8 and 2 K furnishes a Sommerfeld coefficient (γ_{el} value) of 43 mJ mol^{-1} K^{-2} in UNi_4P_2, which is ~3 times larger than that of the nonmagnetic analog $LuNi_4P_2$ (15 mJ mol^{-1} K^{-2}), while the slopes β_{ph} in the two cases are comparable (0.8 mJ mol^{-1} K^{-4} for UNi_4P_2 and unity in the same units for the Lu analog).

Emphatically, FM order in a pristine 1D Ising chain at a finite temperature is impossible as the entropy (S) term always wins in the free-energy expression $F = E - TS$, where E is the internal energy [19,20]. However, this thermodynamic consideration can be defied by virtue of a local pinning potential, though the experimental realizations are rare. One such scenario has been observed in artificial 1D Ising spins of Co spins where the surface interactions with the Pt substrate provide a pathway to highly unconventional Ising FM order in 1D [14]. For the case of UNi_4P_2 the anisotropic cf hybridization provides the local pinning potential. Figures 2 and 4 and Table I clearly illustrate this.

By analysis of the $M(H)$ curves near T_{Curie}, we deduce the critical exponents $\beta = 0.205$ and $\gamma = 1.513$ (Fig. 6) assuming the Arrott-Noakes equation of state, $(H/M)^{1/\gamma} = (T - T_{Curie})/T_1 + (M/M_1)^{1/\beta}$, in the present case [21]. Here, M_1 is a material-specific parameter. Note that the mean-field exponents ($\beta = 0.5$ and $\gamma = 1$) are found to furnish a curvature as shown in Fig. 6(b) and hence are not applicable here. The exponent γ derived from the Widom scaling law [22] (i.e., $\delta = 1 + \gamma/\beta$) has been used in the inset of Fig. 6(d). The critical exponents of a phase transition depend upon the dimensionality of the lattice and the order parameter and range of interactions involved. To our knowledge, the derived exponents in UNi_4P_2 are unique and may represent 1D Ising-type ferromagnetism stabilized by anisotropic cf hybridization.

Prima facie, the cf hybridization is stronger in UNi_4P_2 compared with that in the Yb analog, especially at higher temperatures, as the magnetic anisotropy in $YbNi_4P_2$ weakens significantly above 10 K following free-ion-like Curie-Weiss behavior furnishing $\mu_{eff} = 4.54\ \mu_B$, a value close to that expected for Yb^{3+}, in stark contrast with UNi_4P_2, where the experimental μ_{eff} values are lower than the single-ion val-

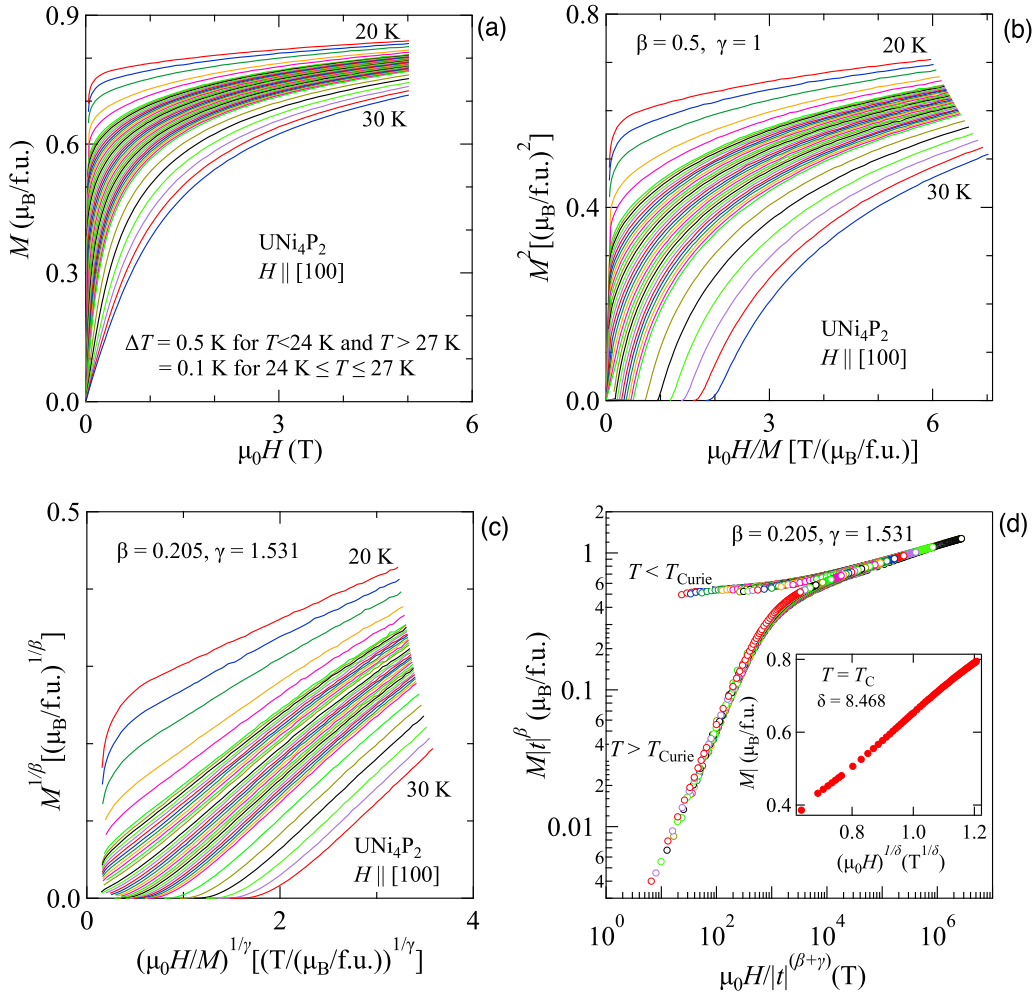

FIG. 6. Critical exponent analysis of the ferromagnetic order in UNi_4P_2. (a) Magnetization isotherm in the vicinity of T_{Curie}, (b) Arrott plot (cf. $\beta = 0.5$ and $\gamma = 1$ in the mean-field model), and (c) Arrott-Noakes plot with $\beta = 0.205$ and $\gamma = 1.513$ found to describe best the critical behavior. The same exponents are used for the scaling analysis in (d). Here, t is the reduced temperature defined as $t = T/T_{Curie} - 1$.

ues, i.e., 3.62 and 3.58 μ_B/f.u. corresponding to U^{3+} and U^{4+}, respectively [10,11]. This happens despite a very small entropy released up to T_{Curie} and very small value of the ordered moment in $YbNi_4P_2$. Furthermore, though the magnetic anisotropy is apparently identical in the ordered state for the two materials, soon after T_{Curie}, there is a reversal in anisotropic direction for the Yb analog. A simple explanation could be that the cf hybridization drives the f moments to lie in the basal plane as it makes the overall configuration of the system energetically favorable. Then, the reversal of the easy magnetization axis in $YbNi_4P_2$ can be understood by its strongly hybridized ground state that weakens rapidly with temperature.

Another understanding which UNi_4P_2 can provide is pertinent to the family of ferromagnetic superconductors, namely, URhGe, UCoGe, UGe_2, and UTe_2 [23]. It has been proposed that the Ising character of the magnetic fluctuations has a crucial role in the unconventional superconducting states. Also, in all the cases where it is possible, itinerant metamagnetic transitions (MMTs) occur for transverse magnetic fields applied in the hard magnetization axis, along which the magnetic susceptibility is largest. Dramatically, the magnetic fluctuations close to such a MMT enhance the effective mass of the conduction electrons, which in turn pair up to form a highly unconventional field reentrant superconducting state. The absence of such a phenomenon in UNi_4P_2 indicates that either the dimensionality of the magnetism is a crucial parameter in addition to Ising-type anisotropy in the reentrant superconducting state or 57 T is not enough for UNi_4P_2 to develop an induced moment along the c axis to surmount the spontaneous magnetization in the a axis, or both. To confirm or rule out the second situation (that 57 T is not enough), we propose a higher-field magnetization measurement in UNi_4P_2 for $H \parallel c$.

One more phenomenological trend connecting the shortest U-U distance with anisotropy in hybridization which, in turn, is related to anisotropic exchange in ferromagnets is highlighted in Ref. [23]. According to Ref. [23], (i) there is a stronger hybridization in the direction of the shortest U-U bonds, and (ii) the easy magnetization axis is perpendicular to the shortest U-U bonds. For UNi_4P_2, the second condition is indeed met, but the first one is not. The obvious reason for this disagreement is that the density of conduction electrons available for hybridization with the $5f$ moments is highest in the basal plane, while negligible in the direction of the shortest U-U distance, i.e., the c axis.

In conclusion, UNi_4P_2 presents astounding physics which this uranium material can host at the intersection of cf hybridization and low dimensionality together with ferromagnetism in the presence of electron correlations.

We thank Prof. Y. Ōnuki for fruitful discussions. We acknowledge financial support from KAKENHI Grants No. JP15H05882, No. JP15H05886, No. JP15K21732, No. JP15H05884, No. JP19H00646, No. JP19J20539, No. JP18F18017, No. JP17K14328, No. JP20K03854, and No. JP20K03851. A. Maurya acknowledges J-Physics, JSPS, and IMR for support through their international fellowship programs. This work is partly supported by funds for collaborative research for shared use of large-scale facilities of Institute for Solid State Physics (ISSP), The University of Tokyo.

[1] D. Aoki and J. Flouquet, J. Phys. Soc. Jpn. **83**, 061011 (2014), and references therein.
[2] J. A. Mydosh, P. M. Oppeneer, and P. S. Riseborough, J. Phys.: Condens. Matter **32**, 143002 (2020), and references therein.
[3] S. Ran, C. Eckberg, Q. P. Ding, Y. Furukawa, T. Metz, S. R. Saha, I. Liu, M. Zic, H. Kim, J. Paglione, and N. P. Butch, Science **365**, 684 (2019).
[4] D. Aoki, A. Nakamura, F. Honda, D. X. Li, Y. Homma, Y. Shimizu, Y. J. Sato, G. Knebel, J.-P. Brison, A. Pourret, D. Braithwaite, G. Lapertot, Q. Niu, M. Vališka, H. Harima, and J. Flouquet, J. Phys. Soc. Jpn. **88**, 043702 (2019).
[5] Y. Shimizu, A. Miyake, A. Maurya, F. Honda, A. Nakamura, Y. J. Sato, D. X. Li, Y. Homma, M. Yokoyama, Y. Tokunaga, M. Tokunaga, and D. Aoki, Phys. Rev. B **102**, 134411 (2020).
[6] A. Maurya, D. Bhoi, F. Honda, Y. Shimizu, A. Nakamura, Y. J. Sato, D. X. Li, Y. Homma, M. Sathiskumar, J. Gouchi, Y. Uwatoko, and D. Aoki, Phys. Rev. B **104**, 195119 (2021).
[7] A. Steppke, R. Küchler, S. Lausberg, E. Lengyel, L. Steinke, R. Borth, T. Lühmann, C. Krellner, M. Nicklas, C. Geibel, F. Steglich, and M. Brando, Science **339**, 933 (2013).
[8] T. Ebel, J. H. Albering, and W. Jeitschko, J. Alloys Compd. **266**, 71 (1998).
[9] C. Krellner, S. Lausberg, A. Steppke, M. Brando, L. Pedrero, H. Pfau, S. Tence, H. Rosner, F. Steglich, and C. Geibel, New J. Phys. **13**, 103014 (2011).
[10] C. Krellner and C. Geibel, J. Phys.: Conf. Ser. **391**, 012032 (2012).
[11] V. Sechovsky and L. Havela, in *Handbook of Magnetic Materials*, edited by K. H. J. Buschow (Elsevier, New York, 1998), Vol. 11, Chap. 1, pp. 1–289.
[12] Y. Onuki, *Physics of Heavy Fermions: Heavy Fermions and Strongly Correlated Electrons Systems* (World Scientific, Singapore, 2018).
[13] D. Gignoux and J. C. Gomez-Sal, Phys. Rev. B **30**, 3967 (1984).
[14] P. Gambardella, A. Dallmeyer, K. Maiti, M. C. Malagoli, W. Eberhardt, K. Kern, and C. Carbone, Nature (London) **416**, 301 (2002).
[15] E. P. Wohlfarth, J. Magn. Magn. Mater. **7**, 113 (1978).
[16] Y. Takahashi, *Spin Fluctuations Theory of Itinerant Electron Magnetism* (Springer, New York, 2013).
[17] N. Tateiwa, J. Pospisil, Y. Haga, H. Sakai, T. D. Matsuda, and E. Yamamoto, Phys. Rev. B **96**, 035125 (2017).
[18] N. Tateiwa, Y. Haga, and E. Yamamoto, Phys. Rev. B **99**, 094417 (2019).
[19] S. Blundell, in *Magnetism in Condensed Matter* (Oxford University Press, Oxford, 2001), Chap. 6, pp. 111–140.
[20] N. D. Mermin and H. Wagner, Phys. Rev. Lett. **17**, 1133 (1966).
[21] A. Arrott and J. E. Noakes, Phys. Rev. Lett. **19**, 786 (1967).
[22] B. Widom, J. Chem. Phys. **43**, 3892 (1965).
[23] R. A. Robinson, A. C. Lawson, V. Sechovsky, L. Havela, Y. Kergadallan, H. Nakotte, and F. R. de Boer, J. Alloys Compd. **213-214**, 528 (1994).